Archives of Acoustics Vol. 48, No. 2, pp. 191–199 (2023), doi: 10.24425/aoa.2023.145230

Research Paper

Infrasound Signal Classification Based on ICA and SVM

Quanbo LU, Meng WANG, Mei LI*

School of Information Engineering, China University of Geosciences
Beijing, China

*Corresponding Author e-mail: maggieli@cugb.edu.cn

(*received July 7, 2022; accepted December 7, 2022*)

A diagnostic technique based on independent component analysis (ICA), fast Fourier transform (FFT), and support vector machine (SVM) is suggested for effectively extracting signal features in infrasound signal monitoring. Firstly, ICA is proposed to separate the source signals of mixed infrasound sources. Secondly, FFT is used to obtain the feature vectors of infrasound signals. Finally, SVM is used to classify the extracted feature vectors. The approach integrates the advantages of ICA in signal separation and FFT to extract the feature vectors. An experiment is conducted to verify the benefits of the proposed approach. The experiment results demonstrate that the classification accuracy is above 98.52% and the run time is only 2.1 seconds. Therefore, the proposed strategy is beneficial in enhancing geophysical monitoring performance.

Keywords: independent component analysis; fast Fourier transform; support vector machine; infrasound signal.

1. Introduction

Infrasound (generally less than 20 Hz) is a low-frequency sound produced by natural and anthropogenic events. The frequency of infrasound signals typically is under 20 Hz (Gi, Brown, 2017; McKee *et al.*, 2018). Although it cannot be heard by the human auditory system, it widely exists in the world around us. Infrasound can be produced by natural events such as earthquakes, tsunamis, mudslides, tornadoes, and volcano eruptions (Liu *et al.*, 2021). Human induced events such as missile launches, ship navigation, and nuclear explosions can produce infrasound (Zhao *et al.*, 2021). Infrasound is low frequency, long wavelength sound wave, accessible to diffraction, and not easily absorbed by the medium (Mayer *et al.*, 2020; Cárdenas-Peña *et al.*, 2013; Cannata *et al.*, 2011). Therefore, infrasound can be employed in natural disaster monitoring.

Some scholars study infrasound signal classification algorithms and apply them to monitor infrasound signals. Thüring *et al.* (2015) classified the infrasound data from the avalanche control site near Lavin in the Swiss Alps via SVM. The false detection rate was reduced from 65% to 10%, and the classification performance was significantly improved. Reliable help was provided for establishing the automatic detection system of infrasound avalanche (Iezzi *et al.*, 2019). Tsybul'skaya *et al.* (2012) classified atmospheric infrasonic signals based on the theory of testing statistical hypotheses. HAM *et al.* (2008) used radial basis function (RBF) network as the subnetworks of parallel neural network classifier bank to classify six different infrasound events. The classification accuracy reached more than 93%. Through data mining classification algorithms, the feature extraction can be conducted on the signal to achieve a better classification. Liu *et al.* (2014) used three types of feature extraction techniques (spectral entropy, discrete wavelet transformation (DWT), and Hilbert-Huang transform (HHT)) to extract the feature vector of four types of infrasound signals. The signal feature was extracted by back propagation neural network and SVM for classification. As a result, SVM has a greater classification accuracy (Li *et al.*, 2016). However, these methods do not separate the signal from the noise, which may limit their accuracy.

This research provides an approach for monitoring infrasound signal. The proposed technique first applies a blind source separation (BSS) method based on ICA to extract useful signals from mixed infrasound sig-

nals. Then fast Fourier transform (FFT) is carried out for feature extraction. Finally, SVM is utilized to classify the infrasound signals based on the retrieved features. The infrasound signal experiment is conducted to validate the superiority of our proposed technique. It provides a practical mechanism for real-time monitoring and analysis of infrasound signals (Chernogor, Shevelev, 2018).

The remainder of this work is organized as follows. The methodologies and algorithms used in this paper are briefly discussed in Sec. 2. In Sec. 3, the performance of the proposed approach is compared in an experiment. Section 4 shows the experimental results through the analysis of different methods. Finally, conclusions are drawn in Sec. 5.

2. Methods

2.1. Source signal extraction based on independent component analysis

BSS is a well-known concept for separating mixed signals (Sastry *et al.*, 2021). The word "blind" refers to the fact that source signals can be separated even if little information about them is available (Mika, Kleczkowski, 2011). One of the most widely-used examples of BSS is to separate voice signals of people speaking at the same time. This is called the cocktail party problem. This problem aims to detect or extract the sound with a single object even though different sounds in the environment are superimposed on another (Mika, Kleczkowski, 2011). Independent component analysis (ICA) is an analysis method of high-order statistics. It can separate a non-Gaussian characteristic component from mixed signals (Qian *et al.*, 2019). Besides, ICA can remove the aliasing noise from signals without destroying the details. ICA has been applied in many fields and is one of the most powerful tools for data analysis.

As shown in Fig. 1, presenting a linear model of ICA, let $x_1, x_2, ..., x_n$ be an n-dimensional random observation mixed signal, which is a linear combination of $s_1, s_2, ..., s_n$. Each observation $x_i(t)$ is a sample of the random variable. Let the mixed random variables and independent sources have zero mean. The model is defined in matrix form. Let $\mathbf{X} = (x_1, x_2, ..., x_n)^{\mathrm{T}}$ be an n-dimensional random observation vector and $\mathbf{S} = (s_1, s_2, ..., s_m)^{\mathrm{T}}$ be an m-dimensional unknown source signal. Then the ICA can be expressed as:

$$\mathbf{X} = \mathbf{AS} = \sum_{i=1}^{m} a_i s_i, \qquad i = 1, 2, ..., m. \tag{1}$$

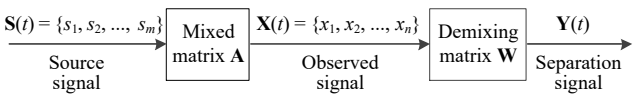

Fig. 1. Linear model of ICA.

Among them, s_i is the independent component, the mixed matrix $\mathbf{A} = [a_1, a_2, ..., a_n]$ is a full rank matrix, and a_i is the base vector of the mixing matrix. In Eq. (1), we can see that each observation data x_i is obtained by the independent source s_i with different a_i linear weighting. The independent source s_i is an implicit variable. It cannot be directly measured. The mixed matrix $\mathbf{A}$ is also an unknown matrix, so the only available information is the observed random vector $\mathbf{X}$. Without any restriction to estimate $\mathbf{S}$ and $\mathbf{A}$ from $\mathbf{X}$, the solution of Eq. (1) must be multiple solutions. However, according to the statistical characteristics of $\mathbf{X}$, ICA will give the unique solution of the equation under certain constraints. The unique solution can extract independent components.

The unknown source signals are independent, which is a fundamental basic assumption. As a result, the probability density function can be written as:

$$p(s) = \prod_{i=1}^{m} p_i(s_i), \tag{2}$$

where $p(s)$ represents the probability density function of the source signal, $p_i(s_i)$ signifies the independent component's probability density function (Mika, Kleczkowski, 2011), s is the source signal, s_i stands for the independent component, and m is chosen as dimension.

The source signals are independent in the ICA model (Mika, Kleczkowski, 2011). The independent signals will have a non-Gaussian distribution. Non-Gaussianity is measured by kurtosis. In order to simplify the model, it is assumed that the unknown mixing matrix $\mathbf{A}$ is a square matrix $m = n$. The purpose of ICA is to find a transformation matrix. The linear transformation $\mathbf{X}$ is used to obtain the n-dimensional output vector:

$$\mathbf{Y} = \mathbf{WX} = \mathbf{WAS}, \tag{3}$$

where $\mathbf{Y}$ is the approximate signal of $\mathbf{S}$, namely $\mathbf{Y} = \widehat{S}$, the initial weight vector for the unmixing matrix $\mathbf{W}$ is arbitrary. However, due to $\mathbf{A}$ and $\mathbf{S}$ being unknown, $\mathbf{Y}$ has two uncertainties (the uncertainty of amplitude of separated signals and the uncertainty of order of separated signals). These uncertainties have no impact on the outcome.

2.2. Fast Fourier transform

Cooley and Tukey (1965) skillfully used the periodicity and symmetry of the $\mathbf{W}_n$ factor to construct a fast algorithm for discrete Fourier transform (DFT), namely FFT. In the following decades, FFT was further developed. At present, the radix-2 and split-radix algorithms are commonly used.

When discussing the mathematical transformation of images, we consider images as functions with two

variables x and y. First, the Fourier transformation of a two-dimensional continuous function is introduced. Let $f(x,y)$ be a function of two independent variables x and y. It satisfies $\int_{-\infty}^{\infty}\int_{-\infty}^{\infty}|f(x,y)|\,\mathrm{d}x\,\mathrm{d}y<0$.

$$F(u,v)=\int_{-\infty}^{\infty}\int_{-\infty}^{\infty}f(x,y)e^{-j2\delta(ux+vy)}\,\mathrm{d}x\,\mathrm{d}y, \quad (4)$$

where $F(u,v)$ is the Fourier transform of $f(x,y)$ and $f(x,y)$ is the inverse Fourier transform:

$$f(x,y)=\int_{-\infty}^{\infty}\int_{-\infty}^{\infty}F(u,v)e^{-j2\delta(ux+vy)}\,\mathrm{d}u\,\mathrm{d}v. \quad (5)$$

The amplitude spectrum, phase spectrum and energy spectrum of the Fourier transform are as follows:

$$|F(u,v)| = [R^2(u,v)+I^2(u,v)]^{1/2}, \quad (6)$$

$$\varphi(u,v) = \operatorname{arctg}[I(u,v)/R(u,v)], \quad (7)$$

$$E(u,v) = R^2(u,v)+I^2(u,v), \quad (8)$$

where $R(u,v)$ and $I(u,v)$ represent the real part and imaginary part of the Fourier transform, respectively.

2.3. Classification using SVM

Cortes and Vapnik (1995) proposed SVM, a pattern recognition method developed based on statistical theory. In order to get the best generalization ability, SVM seeks the optimum balance between model complexity and learning ability based on limited sample information (Amarnath, 2016). In the field of pattern recognition, SVM is mainly employed to handle the challenge of data classification. It demonstrates a number of distinct advantages in solving tiny samples, nonlinear pattern recognition, and high-dimensional pattern recognition (Amarnath, 2016). SVM may be used to solve a wide range of machine learning.

As shown in Fig. 2, the sample C1 is a positive sample, the sample C2 is a negative sample, and a linear function $g(x)=w^Tx+b$ is required to separate C1 from C2. This is the case in two-dimensional space, and in three-dimensional space to separate C1 from C2 a face is required, and in the n-dimensional space an n-1-dimensional hyper-plane is required to be separated. So, the separation of the hyperplane is expressed as:

$$g(x_i)=\left\langle w^T,x_i\right\rangle+b=0. \quad (9)$$

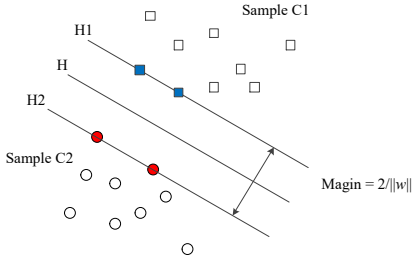

Fig. 2. SVM classification model.

The geometric interval between H1 and H, H2 and H is:

$$d=y_i\cdot\left(w^Tx+b\right)\cdot\frac{1}{\|w\|}. \quad (10)$$

According to Eq. (10), it is necessary to find the nearest point (support vector) of the distance hyperplane in the sample, optimize w and b, and maximize the distance from the support vector to the hyper plane. It is a quadratic programming (QP):

$$\begin{aligned}&\min\frac{1}{2}\|w\|^2\\&\text{subject to }\ y_i\left[\left(w^Tx_i\right)+b\right]-1\geq 0\ \ (i=1,2,...,n).\end{aligned} \quad (11)$$

According to the Lagrange multiplier method, w can be expressed as:

$$w=\alpha_1x_1y_1+\alpha_2x_2y_2+...+\alpha_nx_ny_n=\sum_{i-1}^{n}(\alpha_ix_iy_i), \quad (12)$$

where a_i represents Lagrange multiplier, x_i represents sample points, y_i represents the category label of the i-th sample, and n is the number of samples. In the formula, only the sample point (support vector) belonging to H1 and H2 is not equal to zero, and these non-zero sample points only determine the classification function. Substituting Eq. (12) into Eq. (9) produces:

$$w^Tx+b=\left(\sum_{i=1}^{n}\alpha_iy_ix_i\right)^Tx+b=\sum_{i=1}^{n}\alpha_iy_i\langle x_i,x\rangle+b, \quad (13)$$

where $\langle x_i,x\rangle$ is the Kernel function $K\langle x_i,x\rangle$ of SVM. The Kernel function can convert a sample from a low-dimensional space to a high-dimensional space, allowing it to be separated linearly (Amarnath, 2016). At present, the choice of Kernel function mainly relies on experience. However, because the RBF is preferable in general, the RBF function is chosen as the Kernel function in this research (Chernogor, Shevelev, 2018):

$$K(x,x_i)=\exp\left(-\frac{\left\|x-x_i^2\right\|^2}{\sigma^2}\right). \quad (14)$$

3. Experiment

3.1. Data set and tool

The data used in this paper originates from the International Monitoring System (IMS) with the help of the Comprehensive Nuclear-Test-Ban Treaty Beijing National Data Center (Liu *et al.*, 2014). This study divides infrasound incidents into three types. The data is gathered from sex separate infrasound sensor arrays located all around the world. This study uses 611 sets of data. The details of infrasound data collected from various regions are shown in Table 1. Earthquake,

Table 1. Infrasound data summary.

Event type	Data source (IMS Station Code)	Geographic coordinate	Number of signals	Total	Sampling frequency [Hz]
Earthquake	I14CL	(–33.65, –78.79)	74	203	20
	I30JP	(35.31, 140.31)	124		20
	I59US	(19.59, –155.89)	6		20
Tsunami	I10CA	(50.20, –96.03)	4	218	20
	I22FR	(–22.18, 166.85)	53		20
	I30JP	(35.31, 140.31)	113		20
	I52GB	(–7.38, 72.48)	66		20
Volcano	I30JP	(35.31, 140.31)	189	189	20

tsunami, and volcano eruption are the three types of infrasound events (Li *et al.*, 2016).

All 611 infrasound signal recordings have a sampling frequency of 20 Hz. Figure 3 depicts the infrasound stations' map.

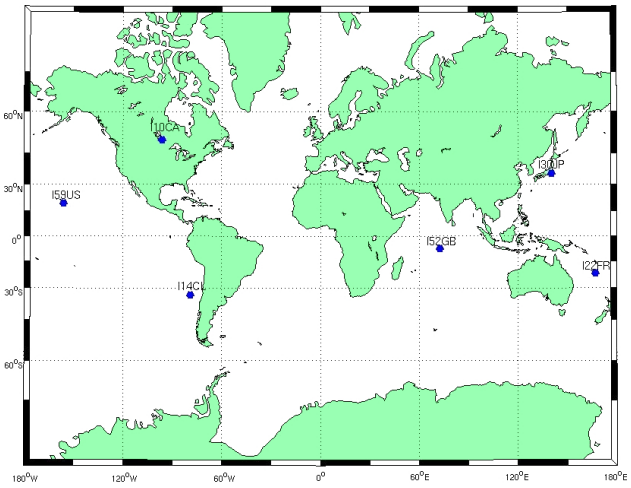

Fig. 3. Map of the infrasound stations.

3.2. Experiment setup

Figure 4 depicts the various categorization model frameworks, while Table 1 contains the data information. Figure 4a shows that the infrasonic signal is transformed by FFT. As a result, the feature extraction obtains three types of feature vectors. Each class is randomly divided into two groups: the training group and the testing group. The proportion of the training group and the testing group is around two to one. The SVM classification model is first trained by the training group. The SVM classification model is next tested by the testing group. Finally, the classification results and accuracy are given. In Fig. 4b ICA is added to remove aliasing noise from the signal without destroying the details of the signal, and then the separated signal is transformed by FFT. As a result, feature extraction obtains three types of feature vectors. Each class is randomly divided into two

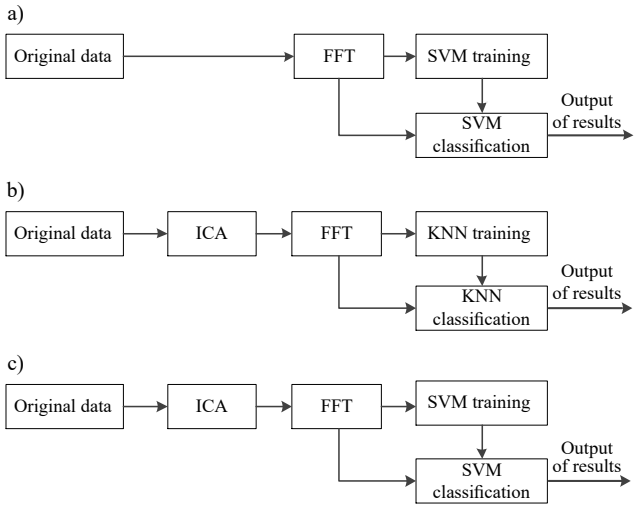

Fig. 4. Classification model framework.

groups: the training group and the testing group. Data from the training group outnumbers data from the test group by around two to one. The K-nearest neighbor (KNN) classification model is first trained by the training group. The KNN classification model is then tested by the testing group. Finally, the classification results and accuracy are given. In Fig. 4c ICA is added to remove aliasing noise in the signal without destroying the details of the signal, and then the separated signal is transformed by FFT. As a result, feature extraction obtains three types of feature vectors. Each class is randomly divided into two groups: the training group and the testing group. Data from the training group outnumbers data from the test group by around two to one. The SVM classification model is first trained by the training group. The SVM classification model is next tested by the testing group. Finally, the classification results and accuracy are given.

3.3. Data preprocessing

The original plot of three infrasonic events is shown in Fig. 5. In Fig. 5, we can see that it is difficult to sep-

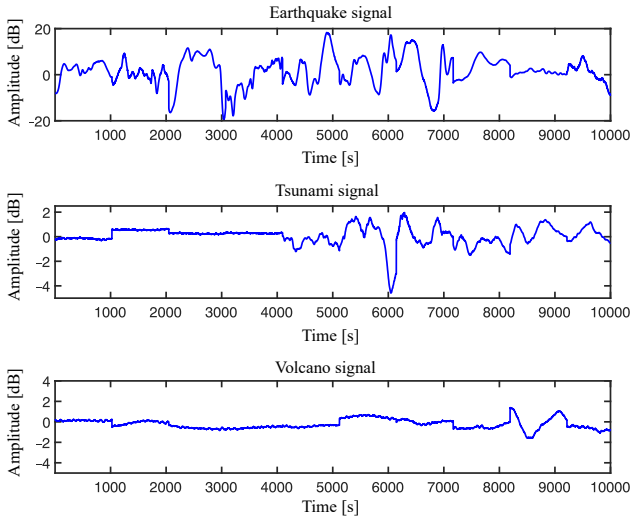

Fig. 5. Original plot of three infrasonic events.

arate different infrasound signals. Therefore, we should extract the feature vectors from the infrasound signal. The feature vectors of three infrasonic events extracted by FFT are presented in Fig. 6. Figure 7 shows the feature vectors of three infrasonic events based on ICA and FFT.

SVM is a supervised classification algorithm. SVM is trained by the training set to obtain the optimal parameters. The final classification result of SVM is obtained by the testing set. The training set data and testing set data of SVM are presented in Table 2. There are 611 infrasound signals, including earthquake, tsunami, and volcano eruption, collected from six infrasound stations. The sampling frequency is 20 Hz. Due to the different lengths of infrasound signals obtained at each infrasound station, all signals need to be truncated, and the data length used in all tests is 1024 points.

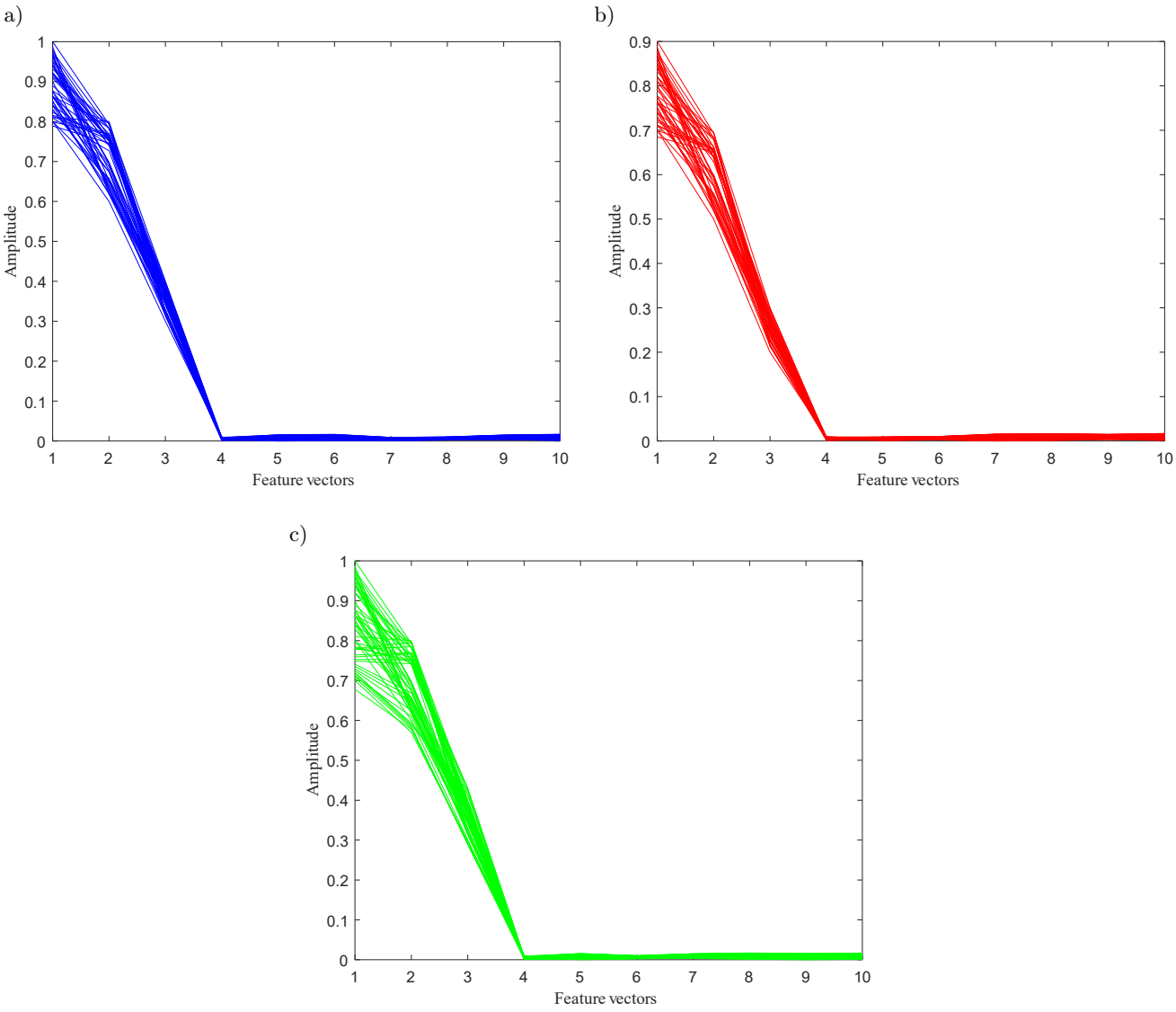

Fig. 6. Feature vectors extracted by FFT: a) feature vectors of earthquake; b) feature vectors of tsunami; c) feature vectors of volcano eruption.

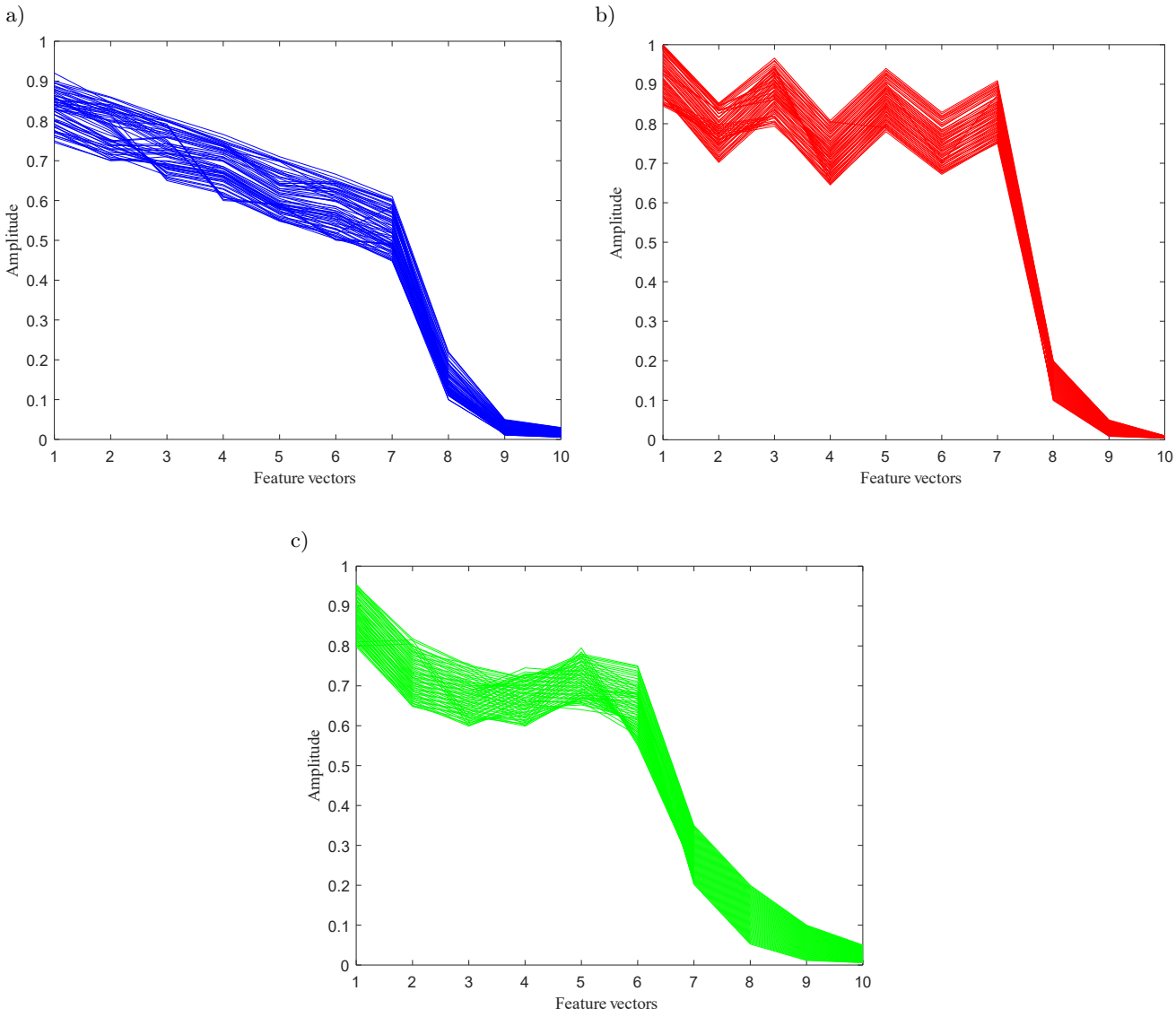

Fig. 7. Feature vectors extracted by ICA and FFT: a) feature vectors of an earthquake; b) feature vectors of a tsunami; c) feature vectors of a volcano eruption.

Table 2. Infrasound classes used for training and testing.

Event type	Class number	Number of vectors	Number of vectors used for training	Number of vectors used for testing
Earthquake	1	204	136	68
Tsunami	2	218	146	72
Volcano	3	189	126	63
Total	–	611	408	203

3.4. Experiment results and discussion

As shown in Fig. 6, the feature vectors of three infrasound events have some similarities. However, there are some differences between them and can be used for infrasound signal classification. Figure 7 shows that the distinction of the feature vectors among different classes is obvious, and the amplitude of the eigenvalues is large. The results show that the proposed methods can extract feature vectors.

The final classification results are shown in Figs. 8 and 9. In these figures, the anticipated label is represented by the abscissa, whereas the true label is depicted by the ordinate.

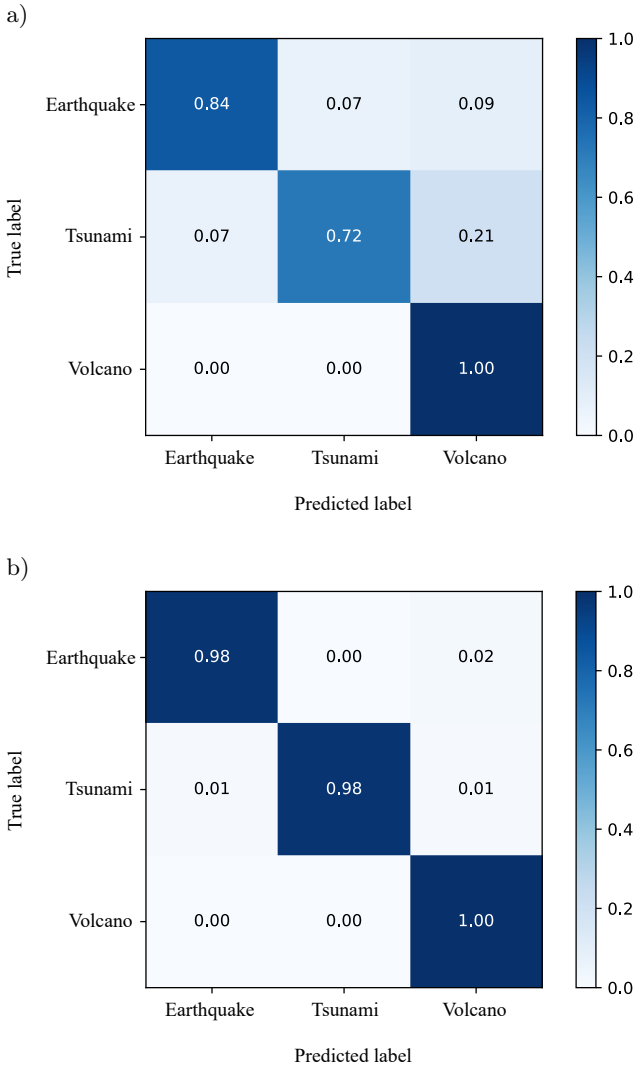

Fig. 8. Confusion matrix of classification results: a) FFT + SVM; b) ICA + FFT + SVM.

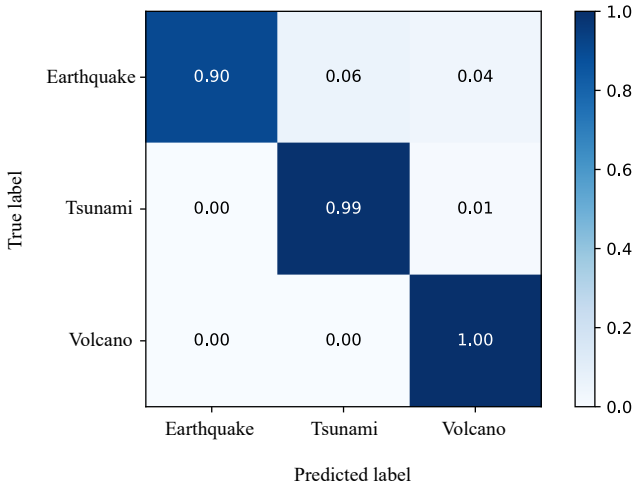

Fig. 9. Confusion matrix of ICA + FFT + KNN classification results.

The confusion matrix of infrasound classification using FFT + SVM is shown in Fig. 8a. The classification accuracy of the three infrasound events is 84.73%. In the classification result of an earthquake by FFT + SVM, five earthquake feature vectors are mistakenly identified as tsunami vectors, and six earthquake feature vectors are mistakenly identified as volcano vectors. In the classification result of a tsunami by FFT + SVM, five tsunami feature vectors are mistakenly identified as earthquake feature vectors, and fifteen tsunami feature vectors are mistakenly identified as volcano feature vectors. Some events are misclassified due to similar characteristics.

The confusion matrix of infrasound classification using ICA + FFT + SVM is depicted in Fig. 8b. The classification accuracy of the three infrasound events is 98.52%, according to the results. In the classification result of an earthquake by ICA + FFT + SVM, one earthquake feature vector is mistakenly identified as a volcano feature vector. In the classification result of a tsunami by ICA + FFT + SVM, one tsunami feature vector is mistakenly identified as an earthquake feature vector, and one tsunami feature vector is mistakenly identified as a volcano feature vector. Some events are misclassified due to similar characteristics.

To compare SVM with other methods, we use the ICA + FFT to extract feature vectors from the same data and then use KNN to classify it, as shown in Fig. 9. A comparative test is utilized to verify the efficiency of the proposed method. Compared with FFT + SVM, the classification accuracy of ICA + FFT + SVM increases by 14% and obtains excellent operating speed, as shown in Table 3. This table shows that the classification result of ICA + FFT + SVM is better than ICA + FFT + KNN, which increases by 2% in accuracy and decreases by 1.5 s in run time. This suggests the SVM method is more suitable for classifying the reduced dimension data by ICA.

Table 3. Comparison results of infrasound signal classification.

Classification scheme	Classification accuracy	Run time [s]
FFT combined with SVM	84.73	5.368
ICA and FFT combined with KNN	96.06	3.625
ICA and FFT combined with SVM	98.52	2.124

As shown in Fig. 3, the source locations of the infrasound stations are distributed widely, but their quantity is small. Due to the limitation of the data, the proposed approach may not be generalized for global hazard monitoring.

4. Conclusion and future work

This research presented a reliable approach for classifying and identifying infrasound signals. ICA separated the source signals of mixed infrasound signals, and then the feature vectors of infrasound events were extracted by FFT. Finally, SVM was used to classify the extracted feature vectors. The experiment results can provide practical solutions for the classification of infrasound signals. The study aimed to improve the accuracy of geophysical monitoring. Due to the limitations of the existing conditions, tests can only use small samples and a few infrasound types, which will affect the reliability of the test results. More infrasound data and infrasonic event types must be evaluated in order to obtain more precise results. For future work, real-time infrasound signal classification will be carried out, and further studies on infrasound types will be performed. Deep learning should be developed for global infrasound signal classification (Albert, Linville, 2020).

Acknowledgments

This work was supported by the National Natural Science Foundation of China (Grant No. 41572347), 2021 Graduate Innovation Fund Project of China University of Geosciences, Beijing (YB2021YC020). The authors would like to thank the Comprehensive Nuclear-Test-Ban Treaty Beijing National Data Center for providing the data.

References

1. Albert S., Linville L. (2020), Benchmarking current and emerging approaches to infrasound signal classification, *Seismological Research Letters*, **91**(2A): 921–929, doi: 10.1785/0220190116.

2. Amarnath M. (2016), Local fault assessment in a helical geared system via sound and vibration parameters using multiclass SVM classifiers, *Archives of Acoustics*, **41**(3): 559–571, doi: 10.1515/aoa-2016-0054.

3. Cannata A. *et al.* (2011), Clustering and classification of infrasonic events at Mount Etna using pattern recognition techniques, *Geophysical Journal International*, **185**(1): 253–264, doi: 10.1111/j.1365-246X.2011.04951.x.

4. Cárdenas-Peña D., Orozco-Alzate M., Castellanos-Dominguez G. (2013), Selection of time-variant features for earthquake classification at the Nevado-del-Ruiz volcano, *Computers & Geosciences*, **51**: 293–304, doi: 10.1016/j.cageo.2012.08.012.

5. Chernogor L.F., Shevelev N.B. (2018), Characteristics of the infrasound signal generated by Chelyabinsk celestial body: Global statistics, *Radio Physics and Radio Astronomy*, **23**(1): 24–35, doi: 10.15407/rpra23.01.024.

6. Cooley J.W., Tukey J.W. (1965), An algorithm for the machine calculation of complex Fourier series, *Mathematics of Computation*, **19**(90): 297–301, doi: 10.1090/S0025-5718-1965-0178586-1.

7. Cortes C., Vapnik V. (1995), Support-vector networks, *Machine Learning*, **20**: 273–297, doi: 10.1007/BF00994018.

8. Gi N., Brown P. (2017), Refinement of bolide characteristics from infrasound measurements, *Planetary and Space Science*, **143**: 169–181, doi: 10.1016/j.pss.2017.04.021.

9. Ham F.M., Rekab K., Acharyya R., Lee Y.C. (2008), Infrasound signal classification using parallel RBF Neural Networks, *International Journal of Signal and Imaging Systems Engineering*, **1**(3–4): 155–167, doi: 10.1504/IJSISE.2008.026787.

10. Iezzi A.M., Schwaiger H.F., Fee D., Haney M.M. (2019), Application of an updated atmospheric model to explore volcano infrasound propagation and detection in Alaska, *Journal of Volcanology and Geothermal Research,* **371**: 192–205, doi: 10.1016/j.jvolgeores.2018.03.009.

11. Li M., Liu X.Y., Liu X. (2016), Infrasound signal classification based on spectral entropy and support vector machine, *Applied Acoustics*, **113**: 116-120, doi: 10.1016/j.apacoust.2016.06.019.

12. Liu D., Tang D., Zhang S., Leng X., Hu K., He L. (2021), Method for feature analysis and intelligent recognition of infrasound signals of soil landslides, *Bulletin of Engineering Geology and the Environment*, **80**: 917–932, doi: 10.1007/s10064-020-01982-w.

13. Liu X.Y., Li M., Tang W., Wang S.C., Wu X. (2014), A new classification method of infrasound events using Hilbert-Huang transform and support vector machine, *Mathematical Problems in Engineering*, **2014**(3): 1–6, doi: 10.1155/2014/456818.

14. Mayer S., Van Herwijnen A., Ulivieri G., Schweizer J. (2020), Evaluating the performance of an operational infrasound avalanche detection system at three locations in the Swiss Alps during two winter seasons, *Cold Regions Science and Technology*, **173**: 102962, doi: 10.1016/j.coldregions.2019.102962.

15. McKee K., Fee D., Haney M., Matoza R.S., Lyons J. (2018), Infrasound signal detection and back azimuth estimation using ground-coupled airwaves on a seismo-acoustic sensor pair, *Journal of Geophysical Research: Solid Earth*, **123**(8): 6826–6844, doi: 10.1029/2017JB015132.

16. Mika D., Kleczkowski P. (2011), ICA-based single channel audio separation: new bases and measures of distance, *Archives of Acoustics*, **36**(2): 311–331, doi: 10.2478/v10168-011-0024-x.

17. Qian G., Wang L., Wang S., Duan S. (2019), A novel fixed-point algorithm for constrained independent component analysis, *EURASIP Journal on Advances in Signal Processing*, **2019**(1): 28, doi: 10.1186/s13634-019-0622-8.

18. Sastry A.V., Hu A., Heckmann D., Poudel S., Kavvas E., Palsson B.O. (2021), Independent component analysis recovers consistent regulatory signals from disparate datasets, *PLOS Computational Biology*, **17**(2): e1008647, doi: 10.1371/journal.pcbi.1008647.

19. Thüring T., Schoch M., Van Herwijnena A., Schweizer J. (2015), Robust snow avalanche detection using supervised machine learning with infrasonic sensor arrays, *Cold Regions Science and Technology*, **111**: 60–66, doi: 10.1016/j.coldregions.2014.12.014.

20. Tsybul'skaya N.D., Kulichkov S.N., Chulichkov A.I. (2012), Studying possibilities for the classification of infrasonic signals from different sources, *Izvestiya, Atmospheric and Oceanic Physics*, **48**(4): 384–390, doi: 10.1134/S0001433812040147.

21. Zhao J., Liu Y., Yang J. (2021), 3D matching positioning method for landslide using infrasound signal received by triangular pyramid vector array, based on ray theory, *Bulletin of Engineering Geology and the Environment*, **80**(2): 889–904, doi: 10.1007/s10064-020-01988-4.